Article

Not peer-reviewed version

Range and Depth Estimates of Whale Signals Recorded by Triplets of Hydrophones

Ronan Le Bras * and Peter Nielsen

Posted Date: 15 October 2024

doi: 10.20944/preprints202410.1227.v1

Keywords: hydro acoustics; signal processing; location methods

 doi:10.20944/preprints202410.1227.v1

Article

Range and Depth Estimates of Whale Signals Recorded by Triplets of Hydrophones

Ronan Le Bras [1,*] and Peter Nielsen [2]

[1] Independent Researcher
[2] Independent Researcher; pmlg.nielsen@gmail.com
* Correspondence: ronan.lebras@gmail.com

Abstract: The hydroacoustic in-water stations of the International Monitoring System (IMS) network consist of three hydrophones placed at Sound Fixing and Ranging (SOFAR) channel depths and about 2 km away from each other. Whale signals recorded in the vicinity of a hydrophone triplet offer the opportunity to verify simple models of propagation in the immediate neighborhood of the triplet, by comparing arrival times and amplitudes between the three hydrophones. Two examples of whales passing by hydrophone triplets are presented and conclusions drawn about waveform coherency and amplitude of the signals recorded at the three hydrophones in the 0-50 Hz frequency band. On the examples recorded at the HA11 IMS hydroacoustic station, the amplitude decay law of one over the distance is verified, and analysis of hundreds of calls located almost above the hydrophone triplet lead to the possibility that the H11S3 hydrophone may be located further from H11S1 and H11S2, and the H11S1 hydrophone's depth may be deeper than expected from the published locations.

Keywords: hydro acoustics; signal processing; location methods

1. Introduction

Whale songs are frequently observed on the hydrophones of the International Monitoring System (IMS) hydroacoustic network of the Comprehensive Nuclear-Test-Ban Treaty Organization (CTBTO). The larger whales, such as blue whales — Balaenoptera musculus — and fin whales — Balaenoptera physalus — [1], emit acoustic energy in the 15 to 50 Hz range, which can be used to assess simple models of propagation for acoustic waves in the oceans. A lot is unknown about whale vocalization (acoustic signal emitted by whales). Such questions as: the depth at which they emit the sound; the depth-dependent interference of the direct signal with the surface reflection; the possible frequency- and depth- dependent radiation pattern of the acoustic emission. Despite their active nature from the point of view of the whale, they are best classified as passive acoustic noise, as their well-defined and repetitive signals are not under human control. Attempts have been made to estimate the range from the in-water hydrophone IMS stations (a map of the IMS stations is available for viewing and download) at which the signals are observed, as it is well known that acoustic energy can travel very efficiently in the Sound Fixing and Ranging (SOFAR) channel. Five of the six in-water hydrophone IMS stations consist of pairs of triplets of hydrophones close to oceanic islands with one triplet deployed to the north and the other to the south of the island. This is to complement each other in avoiding blockage by the island of energy travelling either from the north or south of the island. The exception is the HA01 station at Cape Leewin, Australia, which consists of a single triplet of hydrophones.

Previous work concerned with whale tracking methods for basic understanding of animal behavior and mitigation of seismic airgun surveys on the animals [2,3], source level of whale signals [4], and population characterization via their acoustic signature [5–8].

Signals from individual (likely) blue whales could be observed in records from January 2003 with a good signal to noise ratio, up to several tens of kilometers from the northern triplet of HA08 in the Chagos archipelago of the Indian ocean [9], using a method based on two parameters — azimuth estimates using the signals on the three hydrophones, and amplitude decay estimates of roughly square-root of the distance — to arrive at their conclusions concerning the range at which

 doi:10.20944/preprints202410.1227.v1

the whale emitted its signal. At these distances, based on modeling up to 250 km, the amplitude of the whale signal decays roughly like the square root of the distance to the hydrophone.

At closer range, it is possible to make the rough assumption that the whale is close to the surface, and then use the differences in the times of arrivals at the three hydrophones to estimate a location. Since the signal does not yet propagate into the SOFAR channel at these distances, the acoustic amplitude should in theory decay as the distance to the hydrophone. This method was used to trace the path of a likely fin whale crossing the waters above hydrophone station HA01, Cape Leeuwin, Australia, [10]. In that work, the authors tracked the progress of the whale through the three hydrophones using the direct arrival from the whale signal. In addition, they observed multiple scattered energy — one directly from the ocean bottom, another from the sea surface after reflection from the ocean bottom — as the whale position was close to being in the area directly above the hydrophones. Figure 1 reproduces the map of the whale track seen on 26 July 2017, at IMS station HA01 [10]. It is computed by assuming that the whale is at the sea surface and using the time differences – estimated via cross-correlation — between the arrivals of individual calls at the three hydrophones organised as a horizontal triplet. The time-annotated yellow dots show the progression of the whale from the south-east of the triplet, directly above hydrophone H01W2, and then out towards the north-west. Figure 1 also shows the envelope of the trace at H01W2, the picks on the envelope, and a section showing four second time intervals of the H01W2 trace after each pick. On the section, scattering from the ocean bottom and the sea surface are clearly visible and cannot be confused with signals from another whale given the move-out of the reflection as the whale passes by the hydrophone. It is also possible that in addition to water reflections, crustal reflections from below the ocean bottom are recorded. Similar multiply scattered arrivals from the ocean bottom and sea surface were observed by Sirovic et al. [11]. In addition to water multiple reflections , crustal reflections were observed from fin whale calls recorded on ocean bottom seismometers in the straights of Juan de Fuca, between the USA and Canada [12].

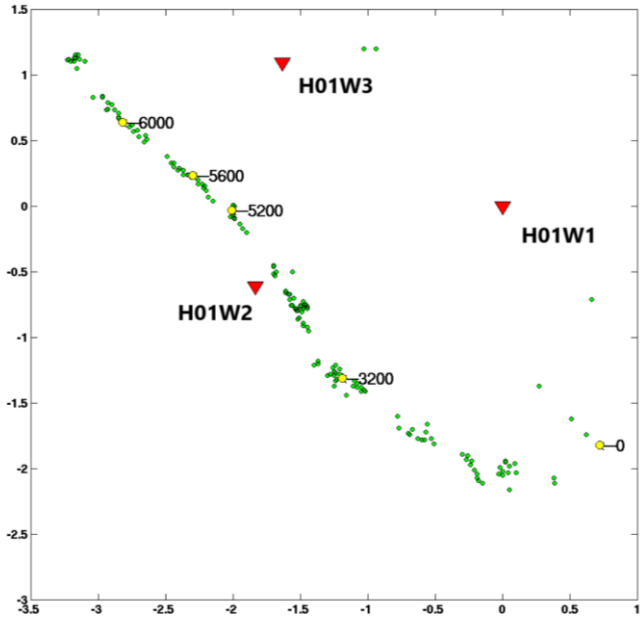

 doi:10.20944/preprints202410.1227.v1

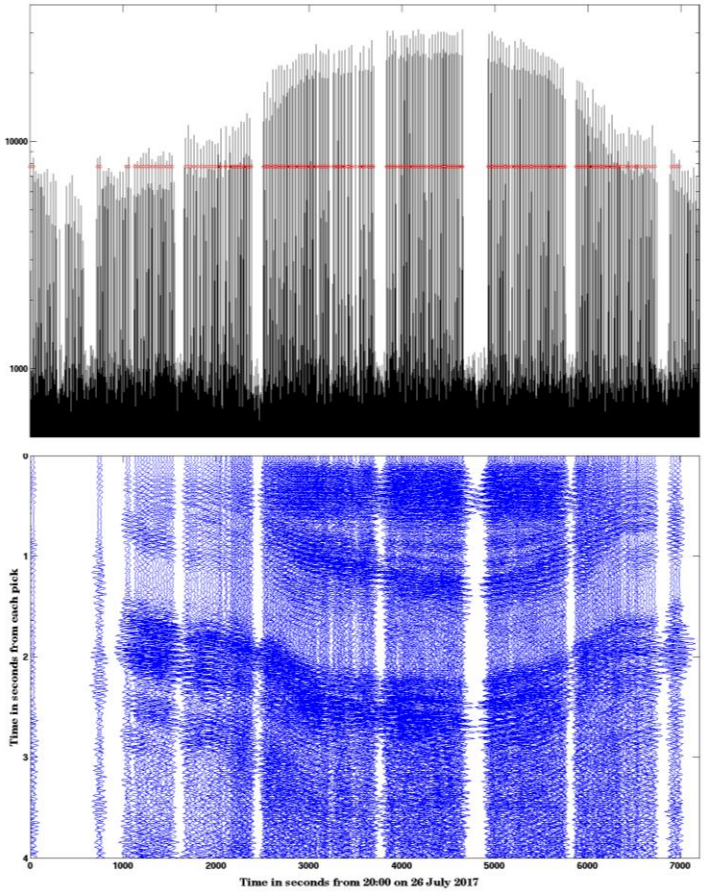

Figure 1. Panel (a) is a map showing the estimated track of the whale as green dots, as it crosses the waters above the three hydrophones of station HA01, at Cape Leeuwin, Australia. The yellow dots overlying some of the green dots, are time-annotated, in seconds after 20:00 UTC on 26 July 2017, which is also time zero of the envelope of the H01W2 trace shown in panel (b). Picks made at the same amplitude level on the envelope are shown as open red circles. Panel (c) is a section made up of four second traces after each pick.

Tagged animal studies [13] have been conducted and show some variability in the swimming depth of a fin whale between very shallow depth (10 m) and up to nearly 300 m. A deeper dive may occur amidst shallower ones. At shallow depths of vocalization of a fin whale, somewhere between the sea surface and 300m depth, it may be difficult to differentiate in time between the direct path from the animal to the hydrophone, and the reflection from the sea surface. A double peak in the autocorrelation and envelope of the first arrival may hint at this sea surface reflection [10]. An elaborate approach [14] based on modeling Lloyd's mirror effect [15] estimated the depth of vocalizing fin whales using the hydrophone and vertical component seismometer channels of Ocean Bottom Seismometers (OBS) and found an estimate of 72 m in one of the examples. Another very interesting paper [16] analyses fin whale vocalization data at the southern triplet of IMS hydroacoustic station HA11. The sequence they analyze is similar to the one used in the work presented here and the authors infer that at least two individual whales are responsible for observed calls with different time-frequency characteristics.The depth of an individual vocalization was also deduced in [16] based on the modeling of travel time at the three hydrophones of the southern triplet of HA11. In this work, data processing and location methods are applied to a data set recorded on the same triplet of IMS hydroacoustic station HA11 on 19 and 20 February 2024, where a likely fin whale passed close to the triplet, like the 26 July 2017 at HA01 reported in [10], and the multiple whales reported in [16]. In addition to [10] and [16], which used only travel times, the presented work also compares observed amplitudes to estimated amplitudes from using a simple model with spherical spreading when whales are known to be at short range directly above a hydrophone triplet.

 doi:10.20944/preprints202410.1227.v1

The next section introduces the 2024 data set, and the methods used to process the data and to find the vocalization locus of a passing whale assuming it is vocalizing at shallow depths. The parameters used in the localization are the time delays between arrivals of the same call at three hydrophones in a triplet. An estimate of the depth of vocalization of the whale when located near two of the hydrophones is made later based on the amplitude ratios of these arrivals and the assumption that the amplitude decays as the inverse of the distance to the hydrophones. Based on a fit of the amplitude ratios for the same signal at the three hydrophones to the ratios of the distances to these hydrophones, an assessment of the values published for the hydrophone location and depths is also made. Applying a correction to these locations would better explain the amplitude data.

2. Data Acquisition and Processing Methods

2.1. Data Acquisition

The data set analyzed in this work was acquired at IMS hydroacoustic stations HA11. Table 1 shows basic site location parameters for the hydrophones of the southern triplet of the station, HA11S.

Table 1. Basic geometry parameters for HA11S triplet. Water depth is 1174m.

Hydrophone	Latitude Longitude* (decimal °)	Depth (m)
H11S1	18.50827 166.700272	739** 750***
H11S2	18.49082 166.705002	739** 742***
H11S3	18.49568 166.686462	739** 724***

* Obtained from [17] **Obtained from [18] ***Obtained from [16].

This data is openly available from the IRIS data center [17] with network code IM. Figure 2 shows two hours of the three hydrophone traces at H11S1, H11S2, and H11S3 at the beginning of the sequence of interest, starting at 21:00 UTC on 19 February 2024. The data of interest is clearly visible on the raw waveform starting at around 22:05 UTC, sixty-five minutes after the beginning of the trace. For the reminder of this work, H11S1 will be referred to as S1, H11S2 as S2, and H11S3 as S3. Several observations can be made regarding the features of the signal on the three waveforms:

- The amplitude of the signal is increasing on all three waveforms starting from about one hour after time zero. This can easily be explained if the source is progressively getting closer to all three sensors until the end of the two-hour sequence.
- The amplitudes at S1 and S3 are slightly higher than at S2.

 doi:10.20944/preprints202410.1227.v1

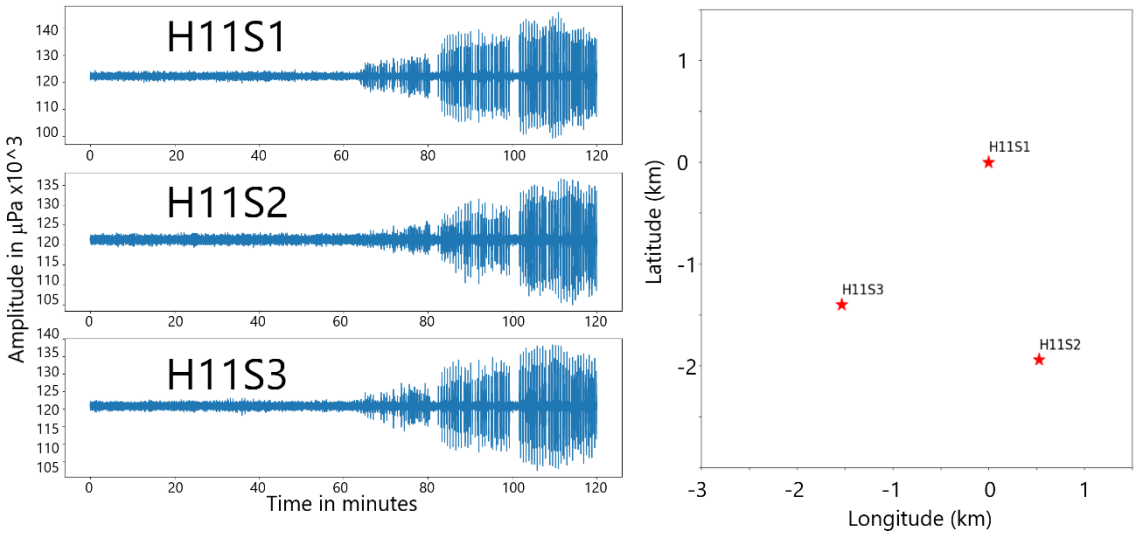

Figure 2. Two hours of hydrophone data starting at 21:00 UTC on 19 February 2024. At the one-hour mark approximately, frequent (roughly once every 25 seconds) impulsive signals are visible and increasing in amplitude towards the end of the section. The time axis is labelled in minutes. The amplitudes are in µPa. The map on the bottom panel shows the basic geometry with the S1 hydrophone being the origin of the local coordinate system. The latitude and longitude differences are in kilometers. The absolute latitude and longitude of the S1 hydrophone are respectively 15.50827 and 166.700272.

There appears to be interruptions of two to three minutes in the sequences of calls at every fifteen to twenty minutes. Since it is well known that cetaceans surface at regular intervals to breathe, it seems natural to infer that these short interruptions correspond to the surfacing of a single individual, or several individuals surfacing in a synchronized fashion, and that the vocalizations happen while the animal dives between the surfacing.

On the spectrogram for the same time interval, the beginning of the trace also shows the large amplitude individual transient arrivals in the 15 to 50 Hz band. This is illustrated by Figure 3 showing the first and last 30 minutes of the two-hour interval. Observations beyond the previous ones can be made from the spectrograms:

- Two types of calls are clearly visible on the spectrogram. One type has a broader bandwidth [17-40Hz] and higher centre frequency than the other one [15-25Hz]. These two types have previously been nomenclatured as type A for the lower frequency type and type B for the higher frequency [16]. The two types are separated by about 25s and generally alternate, but not always. An exception can be seen on Figure 3 in an interval of about 100s after 5600s with three consecutive type B in that interval, and again twice at about 5800s. This has an implication on the measurement of amplitudes, which shows a bimodal distribution as will be shown later in this work.
- If the hypothesis that the interruptions in the calls are at the time of surfacing, the first call when the animal dives is the narrower lower frequency pulse (type A), and the last call is the broader, higher frequency call (type B)

 doi:10.20944/preprints202410.1227.v1

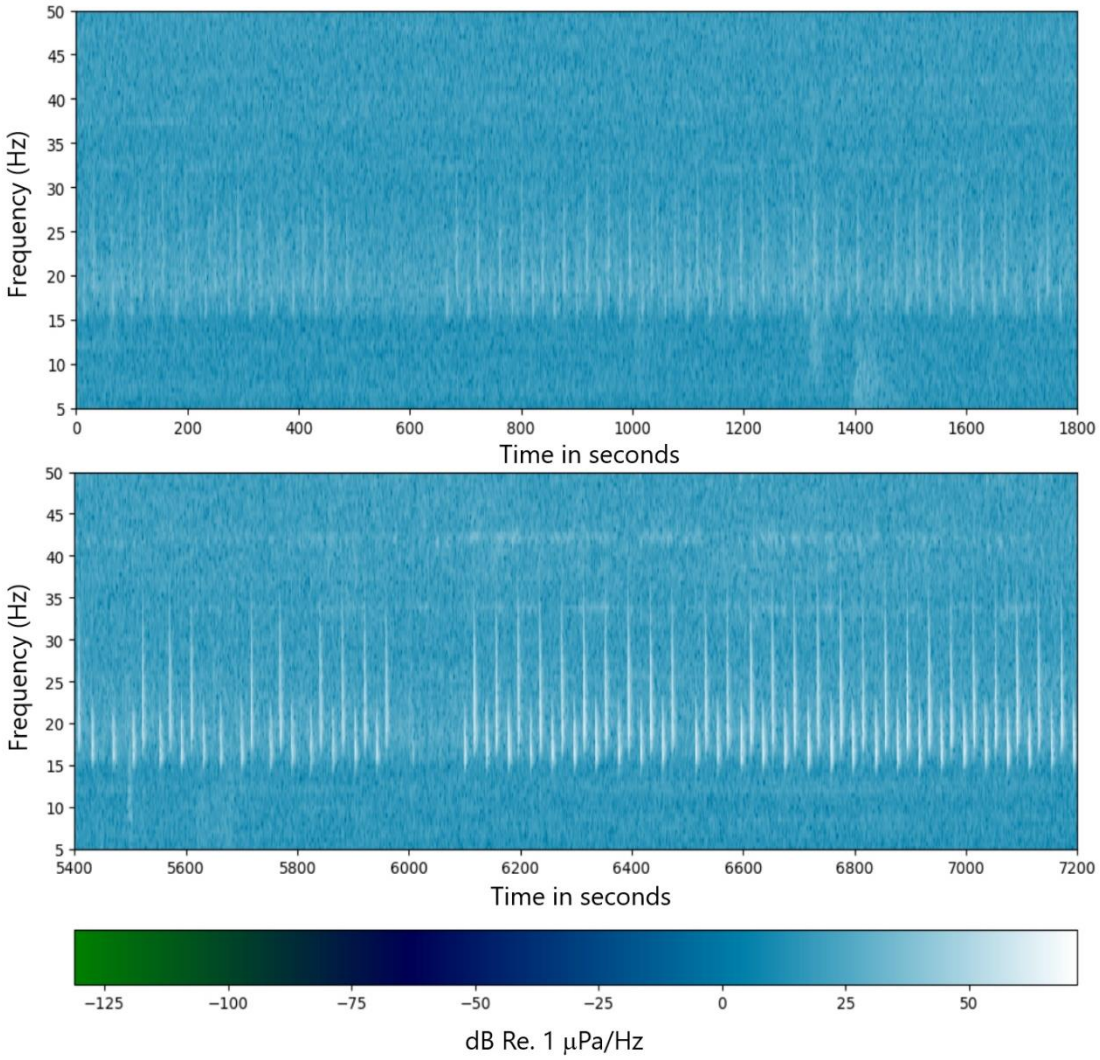

Figure 3. Spectrograms of the first 30 minutes (top) and last thirty minutes (bottom) of the waveforms for S2 shown on Figure 2. The time scale is in seconds.

2.2. Waveform Signal Processing

To assess the location of the whale calls when the signal is strong, we start by picking individual signals out of the background noise using a short-term average to long-term average ratio (STA/LTA) method ([19,20]) with an STA of 0.1s and an LTA of 1s. This method is widely used in seismology and is also part of the hydroacoustic processing chain at the International Data Centre of the CTBTO [21]. In this work, the STA/LTA method is used on the envelope of the waveform after bandpass filtering between 10 and 50 Hz, rather than directly on the waveforms themselves, avoiding the possible confusion between positive and negative maxima. This is illustrated by Figure 4 where values of 5 for the trigger-on and 4 for trigger-off are used on a five-minute segment of data at hydrophone S1 starting at 2:20:00 UTC on the 20 February 2024. Fifteen detections are made in the segment. Figure 4a shows a close-up of the envelope of the first call in the sequence, which is identifed as a type B call. Figure 4b shows the STA/LTA function for that call. For the same time interval, the same number of detections is made on the other two hydrophones (S2 and S3). Figure 4c shows the fifteen calls, with the type identification placed before each call.

Figure 5's panels (a) to (c) show signals for the same call as in Figure 4a at the three hydrophones on 10-second segments starting 2.5 seconds before the on-trigger times at hydrophone S1. Delays between the direct arrivals at the three hydrophones are clearly visible, especially on panel (d) where all three envelopes of the signals are shown on the same plot.

 doi:10.20944/preprints202410.1227.v1

Several methods were tested to compute arrival delays between the three hydrophones to assess a location for the source of the signals in the case when the signal is strong enough to trigger the detector with the parameters specified above:

1. The first method is to compute delays from the cross-correlations between S1 and the other two traces for each detection made at S1. The cross-correlations are computed on ten-second segments and the detection is confirmed on the three traces when the maximum of the cross-correlation is larger than 0.5.
2. The second method is to use detections made on the other hydrophones if they fall within a three-second interval from the S1 detection. The delays are simply the time differences between the detection times.

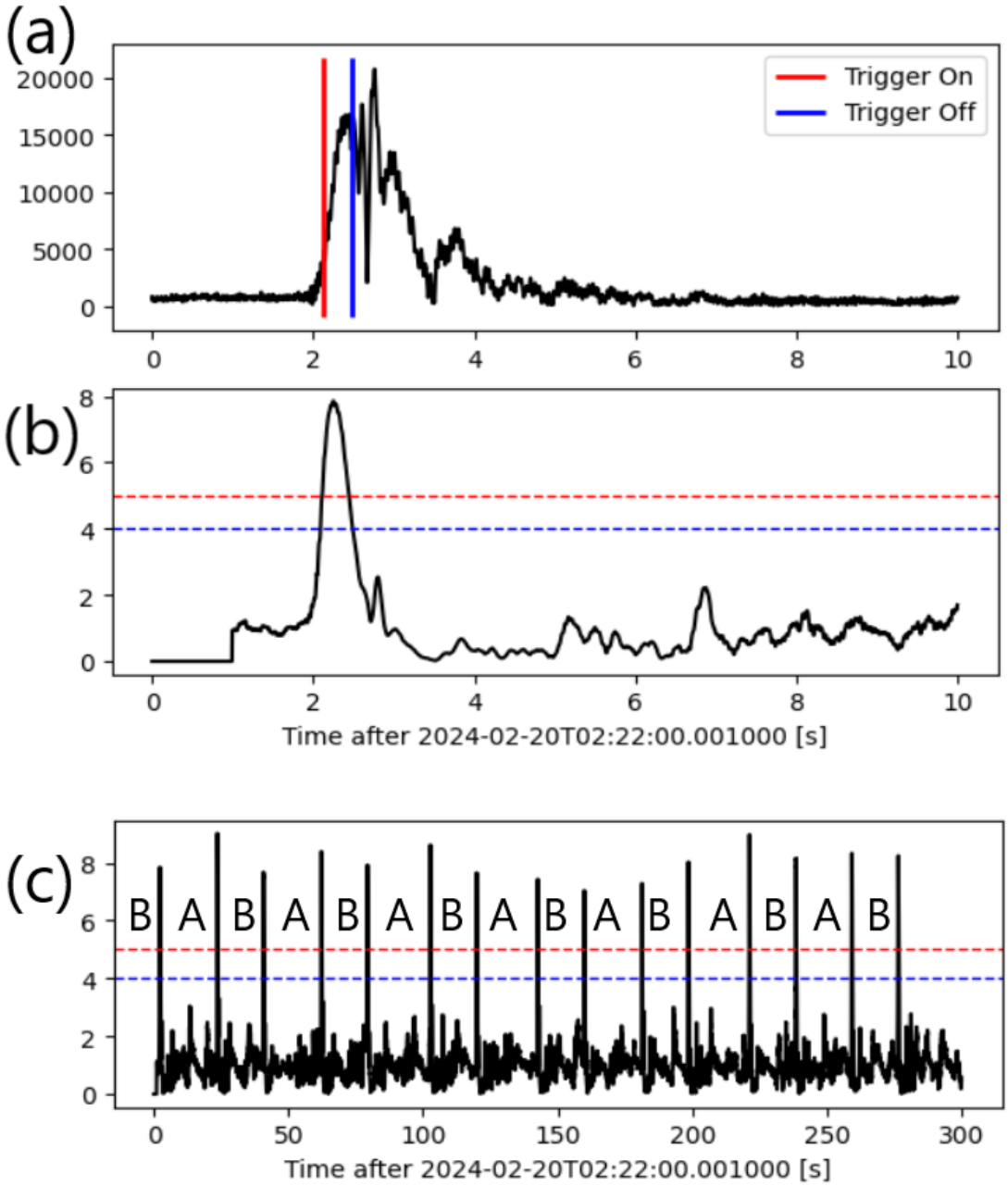

Figure 4. Illustration of the STA/LTA detection method on a 10 second interval (single call) at S1. (a) envelope of the first signal. (b) STA/LTA function of the first signal. (c) Envelope of the five-minute interval with fifteen calls. Each call is labelled 'A' or 'B'. The red vertical markers and dotted lines are respectively the time of the on-trigger detection, for an STA/LTA value of 5 and the blue vertical markers and line the off-trigger times for an STA/LTA value of 4.

Preprints.org (www.preprints.org) | NOT PEER-REVIEWED | Posted: 15 October 2024 doi:10.20944/preprints202410.1227.v1

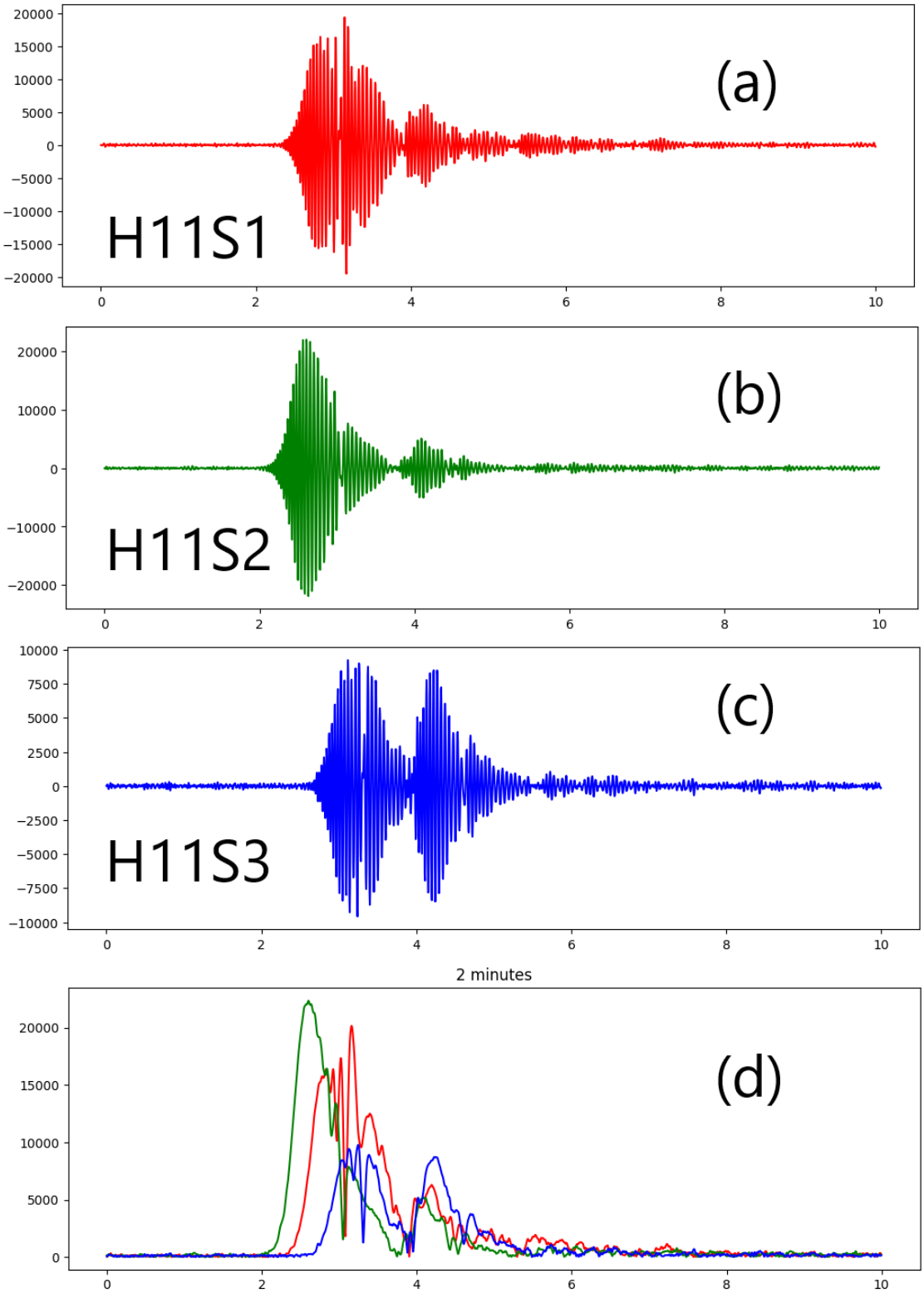

Figure 5. Panels (a) to (c) are ten-second segments of waveforms for the three hydrophones aligned in the same time scale and the signal at S1 is the same as in Figure 4 at about 2:22:00 on 20 February 2024. Panel (d) shows all envelopes of the panels (a) to (c) using the same color conventions and illustrating the time shifts and amplitude differences.

Figure 6 illustrates the difference in delay computation between the two methods on the two-hour interval shown on Figure 2. The detector found respectively 142, 124, and 131 detections on S1,

 doi:10.20944/preprints202410.1227.v1

S2, and S3 in that interval. Note that the first detection is made after 60 minutes, and it is not until 80 minutes until the end of the two hours that detections are made with high regularity.

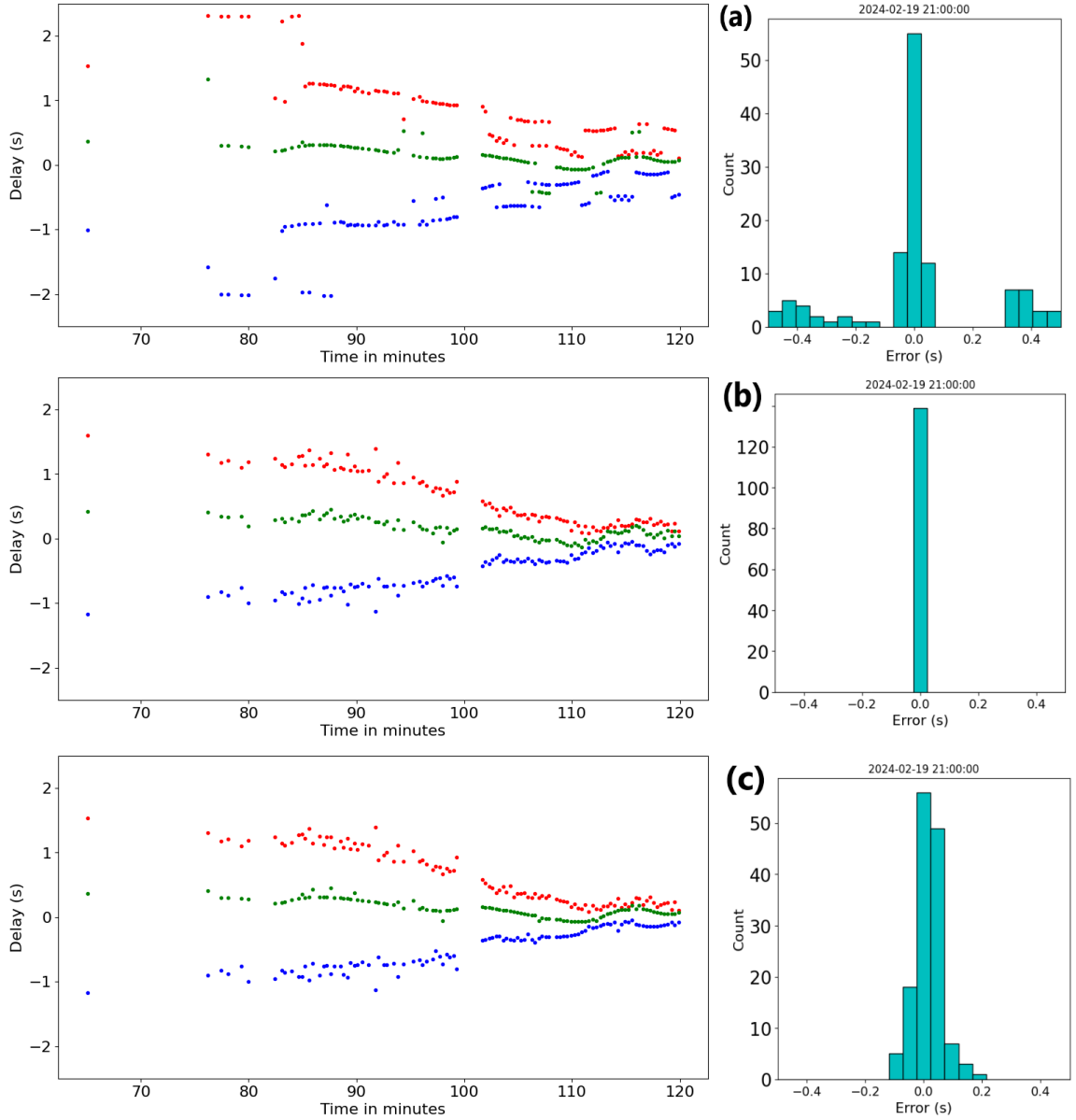

Figure 6. Panel (a) shows the results of picking delay times at S2 and S3 based on method 1 (cross-correlation), and panel (b) is based on method 2 (STA/LTA picks only). Panel (c) shows the result of improved method 2, obtained by adjusting (b) with cross-correlation values when delays are within a tenth of a second of each other. Red dots are the delays (d12) between S1 and S2, the green dots, the delays (d13) between S1 and S3, and the blue dots are the delays between S2 and S3 (d23). On the right of each panel is a histogram of the errors estimated from the difference between the measured delays e = (d23 – (d13-d12)). $|e|$ is called the closure [22].

There are striking differences between the results of the two methods used to compute the delays. The cross-correlation based method 1 (Figure 6a) shows higher consistency between the estimated values of the delay for consecutive calls, however there are sudden jumps in these values from one call to the next. These can be attributed to the reflected arrivals following the first arrival, which can be as large as the first arrival (see for instance S3 trace on Figure 5). The picks-only method 2 (Figure 6b) does not show these sudden jumps in the values of the delays likely because the method ensures that the delays will be computed on the first arrival and not later reflected arrivals. The consistency between two consecutive calls however is not as good as for method 1, partly because there is no warranty that picks based on a value of STA/LTA optimize the alignment of waveforms.

 doi:10.20944/preprints202410.1227.v1

A natural improvement consists of using method 2 to get initial values and then refine the value of the delay via cross-correlation (Figure 6c). In the remainder of this study, it will be referred to as "improved method 2". The histograms on the right of each panel show the distribution of errors for each panel. The errors are always zero by construction for method 2 and can be large for method 1. This may happen for instance when the maximum of the cross-correlation corresponds to a correlation between a direct arrival and a reflected arrival. Improved method 2 shows that introducing a small shift based on the cross-correlation delay values increases the errors. The errors remain within a value of 0.2 seconds, however.

The amplitudes are computed as the maximum of the envelope in a 6s interval starting 3s before the detection trigger time on S1. Figure 7a illustrates the difference in amplitude between the 'A' calls and the 'B' calls. 'B' calls have consistently higher amplitudes. When ratios are considered however, such as the ratio of the amplitude at S1 to the amplitude at S2, types A and B calls show a high degree of consistency. This will allow a comparison of this ratio to the amplitude ratio.

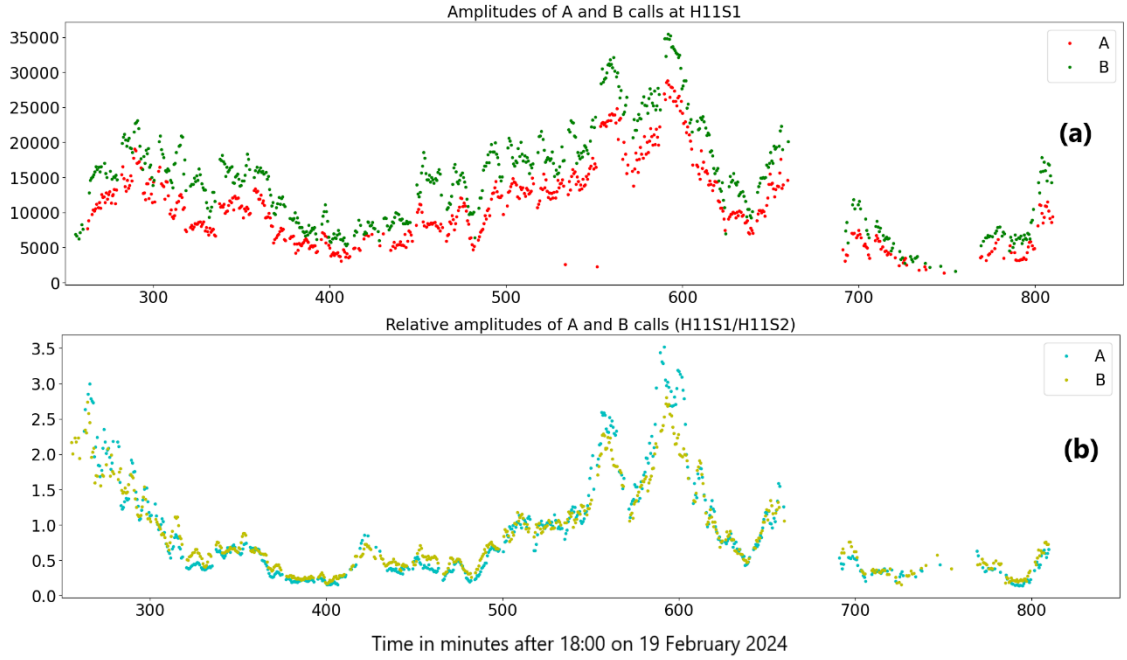

Figure 7. (a) Illustration of the amplitude differences between A and B types of calls. The amplitude measures for type A is consistently higher than for type B. The amplitude scale is in μPa (b) Shows the consistency of the relative amplitudes for types A and B, in this case amplitude at S1 divided by amplitude at S2.

The method described in the previous section works when the calls have sufficient signal to noise ratio (SNR) and are detectable with a power detector method such as STA/LTA. In the absence of sufficient energy at the receiver, it is still possible to obtain the direction of incoming signals using a cross-correlation method on segments of data, with no pre-determined picks, unlike the three methods previously mentioned. For the time preceding the two-hour segment studied so far, the SNR of the signals is very low, but still visible on the spectrograms from about 18:20 UTC. The result of applying these cross-correlations on segments is shown on Figure 8 for the 2 hours and forty-minute period starting at 18:20 UTC and ending at 21:00 UTC and for the 21:00 to 23:00 UTC period previously processed based on STA/LTA picks. Figure 8a shows the spectrogram for the earlier period in the 10-40 Hz frequency band. The computation of the delays is much noisier than it is when the SNR is sufficiently high to warrant a power detector method, as seen on panel 8c, but the back-azimuth can still be estimated from that data and is shown on panel 8e. For comparison with Figure 6, the cross-correlation method on 5s segments is shown on panel 8d. It is quite a bit noisier than any of the panels on Figure 6, but clear trends are seen developing in the second hour of the segment,

 doi:10.20944/preprints202410.1227.v1

with a dominant back-azimuth between 300 and 350 degrees from north, and a hint of another azimuth 180 degrees from it, between 120 and 170 degrees. This latter back-azimuth may be due to back-scattering from the seamount known to underlie the southern triplet of H11A [18]. Panels 8e and 8f clearly show the continuity of the back azimuth between the earlier, low SNR signals and the stronger signals when they reach the vicinity of the triplet of hydrophones. Panels 8g and 8h show the error estimates histograms similarly to Figure 6. It may be possible to use amplitudes to estimate the range, as it would be expected to decay like the square-root of the distance, but this has not been attempted on this data.

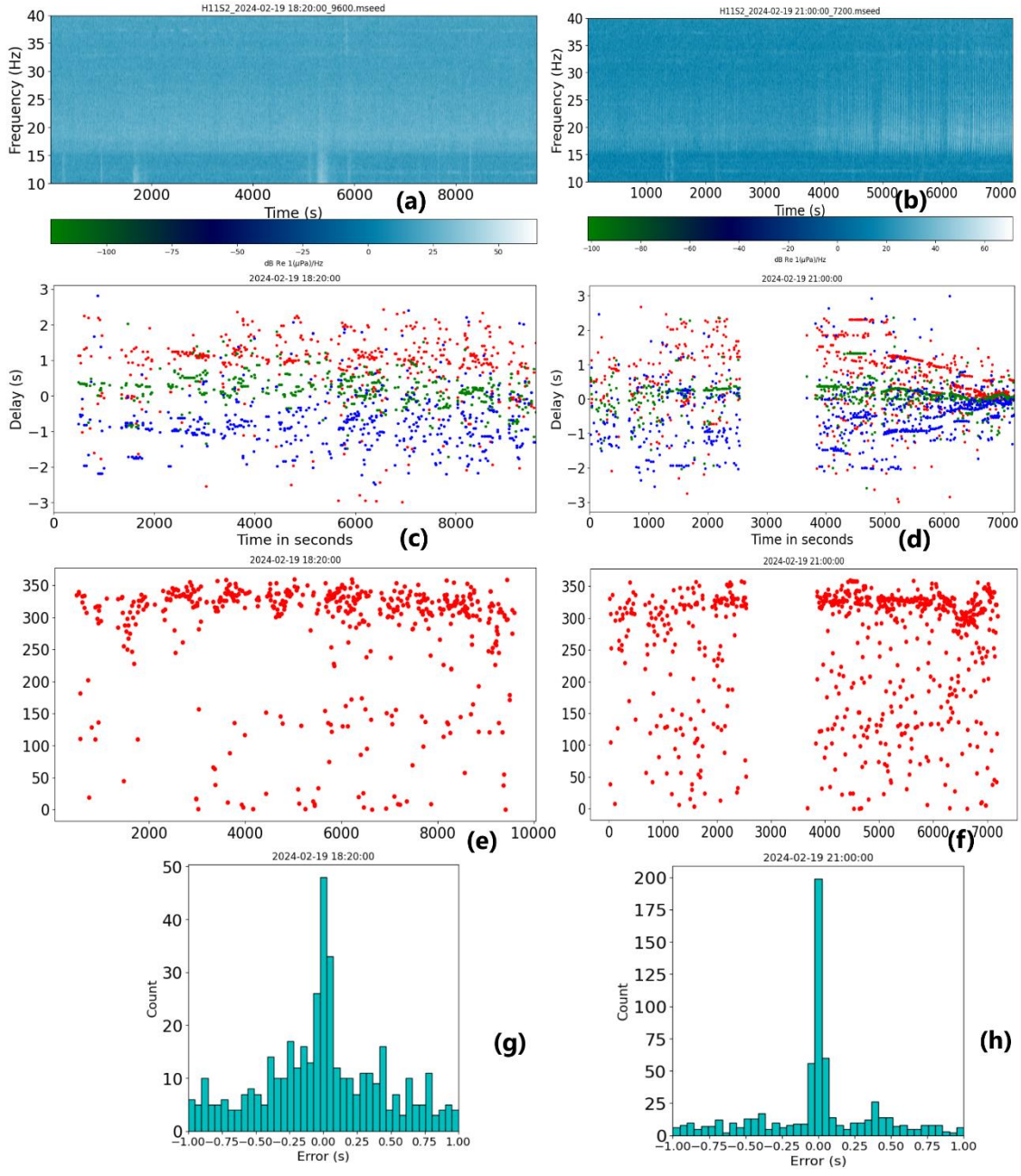

Figure 8. Panels (a) and (b) are the spectrograms for respectively 18:10 to 21:00 and 21:00 to 23:00. Panels (c) and (d) show the results of picking delay times based on cross-correlation on 5s segments with a threshold correlation value of 0.3 for one of the three cross-correlations. The color convention is the same as for Figure 6. Panels (e) and (f) show the back-azimuth estimates for the picks, and panels (g) and (h) are the histograms of error estimates for the respective time intervals.

 doi:10.20944/preprints202410.1227.v1

2.3. Location Method by Grid Search

Since with large amplitudes it is likely that the whale is close to the triplet of hydrophones, we assume straight line propagation and that the whale is close to the surface. The localization of each call is then accomplished by a simple grid search to minimize the time delay differences between measured and modeled delays at each hydrophone, assuming straight ray propagation and a water velocity of 1.48 km/s. The latitude and longitude grid spacing is 25m and the depth difference between the source and receivers is set constant during the search. Specifically, the grid search is initially done over a 12.5 by 12.5 kilometers area to locate the first call. For subsequent calls, the search is limited to an area 2.5 by 2.5 kilometers, since the animal cannot travel far from one call to the next.

3. Results

The location method described above was applied to the data set of 19th and 20th February 2024 and the results are presented in the following sections.

3.1. Location by Grid Search for the Minimum of Root Mean Square (RMS) of Delay Residuals

While the depth at which the whale vocalizes is an unknown, one can assume that it is shallower than the depth of the hydrophones. In a first attempt at tracking the motion of the vocalizing whale, it is assumed to be at the surface of the ocean. Improved method 2, explained in section 2.2 was used to extract the parameters of interest (absolute times of picks, delays between hydrophones, amplitudes of the signal). The amplitudes are computed on the signal's envelopes such as the one shown on Figure 5(d). The depth will trade-off with the projection on the horizontal plane (epicentre in seismology). A way around this is when sensors are directly above the fault in seismology, or directly below the whale for the hydrophones, provided an estimate of the location and origin time are available.

Figure 8 shows a map with the results of the localization of all A calls for the two-hour data set starting at 21:00 UTC on 19 February 2024 (shown on Figure 1). Note the progression of the whale from the northwest to the center of the triplet during this interval. According to [23], both triplets at HA11 were deployed around a seamount. It may not be a coincidence but rather directed by foraging around that seamount that the whale appears to head towards the seamount and to slow down around it. The depth was assumed to be the same for all locations where the whale called.

Preprints.org (www.preprints.org) | NOT PEER-REVIEWED | Posted: 15 October 2024 doi:10.20944/preprints202410.1227.v1

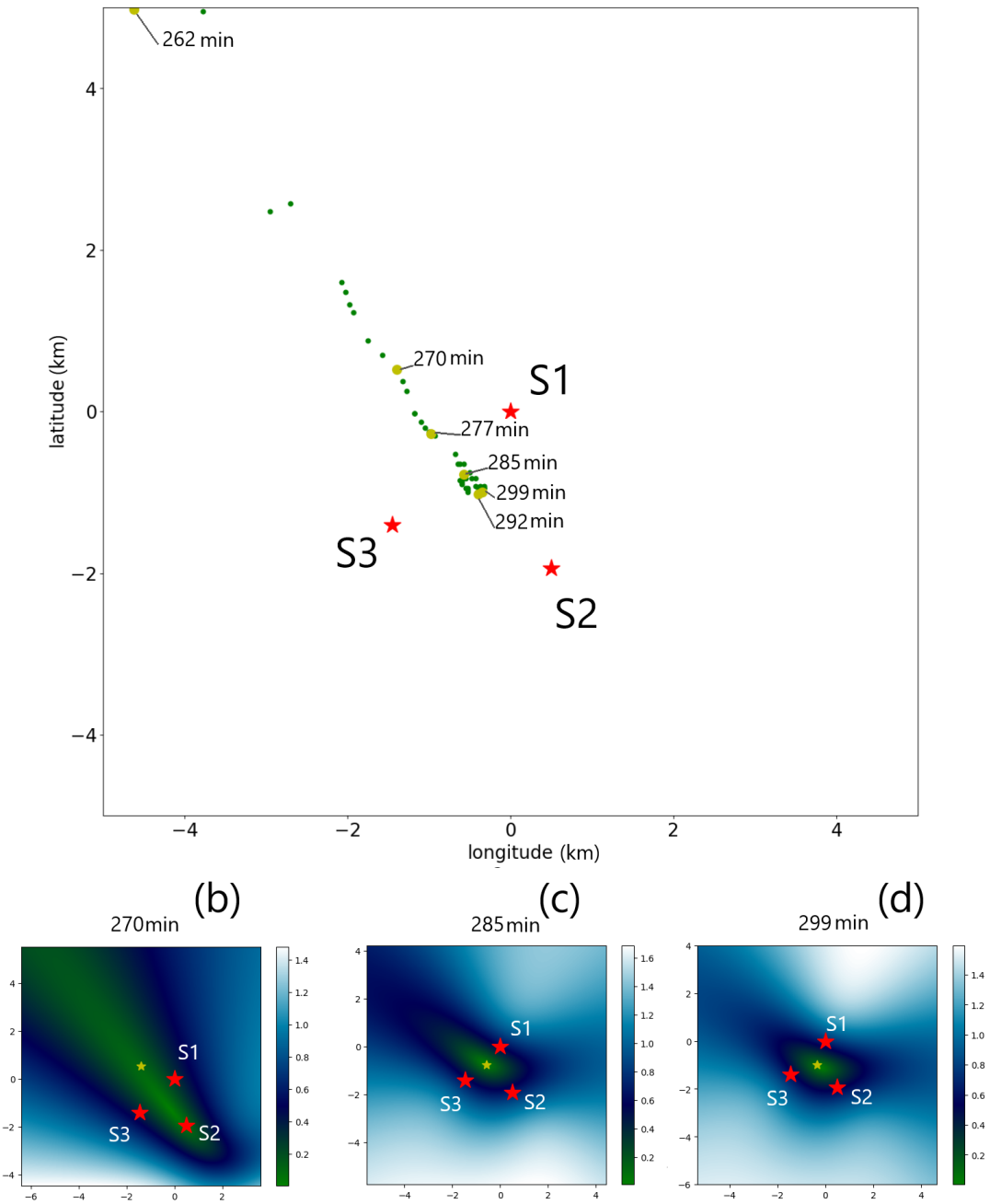

Figure 8. Panel (a) is a map showing the location of all A calls (small green dots). Six of the calls are shown with larger yellow dots and labeled in minutes, corresponding to the detection time on S1 after 18:00 UTC on 19 February 2024, and show the progression of the whale from the northwest of the triplet to its center. The red stars are the locations of the hydrophones. Panel (b) to (d) are the surfaces of the time delay residuals at the time indicated. The yellow star shows the location of the minimum of the RMS of delay residuals for the three specific calls. Note that panels (b) to (d) show ten-kilometers squares centered on the yellow star.

3.2. Using the Amplitude Ratios to Show Possible Corrections Needed to Hydrophone Locations

All calls between 21:00 UTC on 19 February and 14:00 UTC on 20 February with a location close to the center of the hydrophone triplets were gathered into a single data set. A value of 4 for the STA/LTA trigger-on value was used in this case, and a value of 2 for the trigger-off. The assumption that the decay in amplitude is as 1/R also breaks down when the propagation becomes horizontal. As demonstrated on Figure 8, the uncertainty on the location of a call is greater when the whale is outside of the perimeter of the triplets. This is also reflected in the average distance between consecutive calls

 doi:10.20944/preprints202410.1227.v1

as shown on Figure 9. The yellow line is the distance of the location of calls to the center of the triplet. When that distance falls below 1.5 km, shown by the solid black line, the distance between consecutive calls is concentrated around or below 0.25 km, indicating that a more accurate location is obtained inside of the circle of 1.5 km.

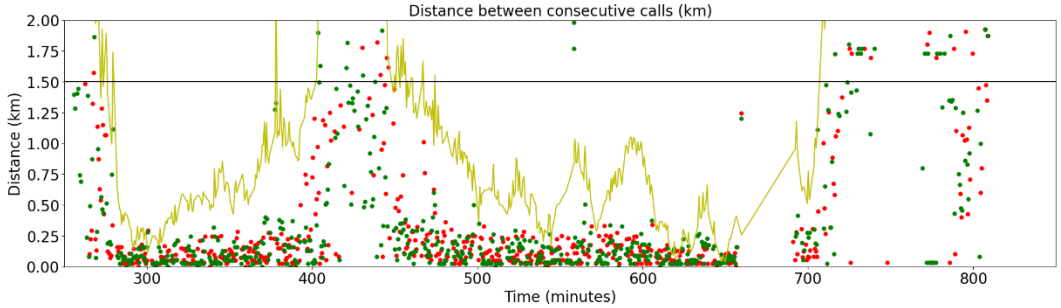

Figure 9. Based on the location derived from the time delays for the A and B calls, the distance between consecutive calls of the same type are shown on this graph. The red dot correspond to the A calls and the green dots to the B calls. The yellow line is the distance from the B calls to the centre of the triplet. Since the A and B calls are close to each other, the line derived from the A calls would be very similar. The solid black constant line shows a value of 1.5 km for that distance.

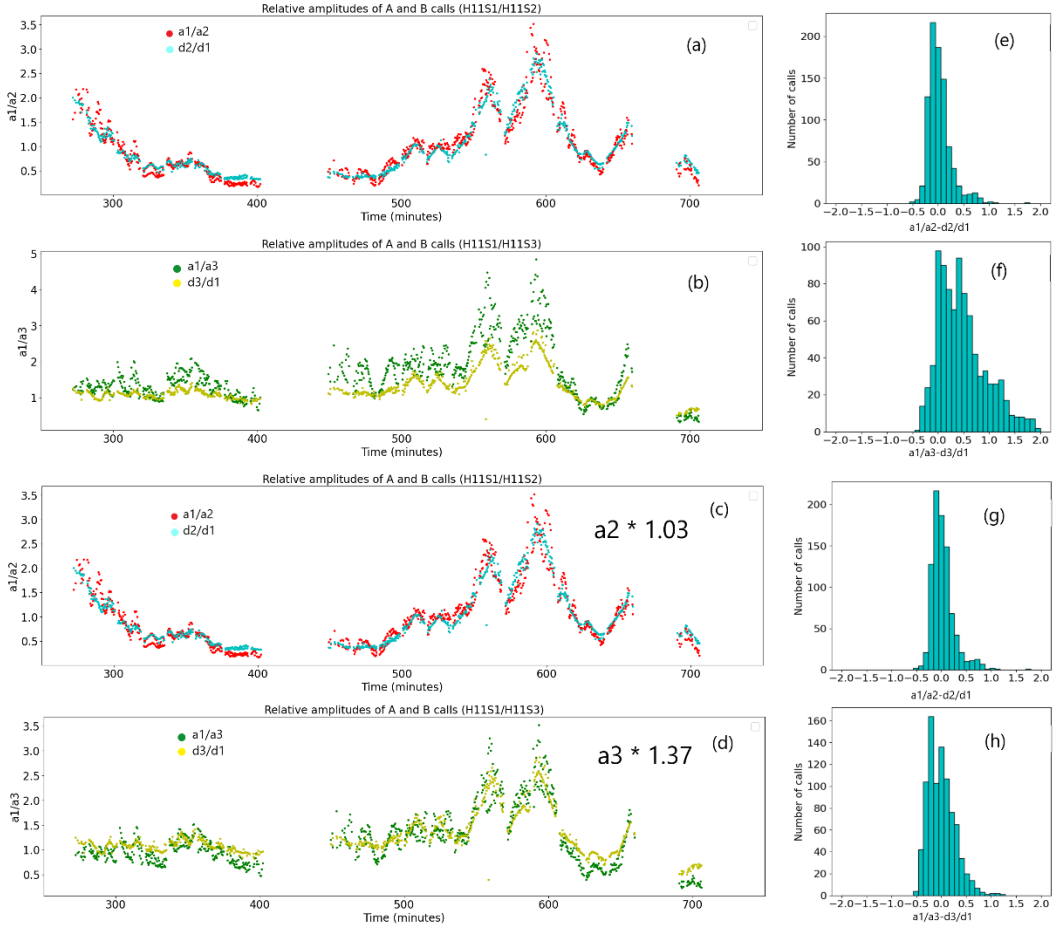

Figure 10. Relative measured amplitudes a1/a2 (a) and a1/a3 (b) displayed as a function of time when the call location is within 1.5 km of the triplet centre. The scale is in minutes from 18:00 on 19 February 2024. For comparison, the distance ratios d2/d1 and d3/d1 are displayed on the same graphs. When a constant bias of 1.03 and 1.375 are applied to respectively a2 and a3, the graphs are displayed in (c) and (d). The histograms of the residuals (a1/a2-d2/d1) and (a1/a3-d3/d1) corresponding to each time series are shown to their right in (e), (f), (g), and (h).

 doi:10.20944/preprints202410.1227.v1

The relative amplitudes were discussed in section 2.2, and it was concluded that the A and B calls, while exhibiting different absolute amplitudes in the frequency band considered, the relative amplitudes between hydrophones show consistency between the two types of calls. Figure 10 shows the variations and histograms of the relative amplitudes a1/a2 and a1/a3 where a1, a2, a3 are respectively the amplitudes measured at S1, S2, and S3.

The measured (a1/a2) and theoretical (d2/d1) values follow each other quite closely, while a1/a3 and d3/d1 depart from each other, as emphasized by the histogram of the difference. When a simple constant bias value, computed as the ratio of the average of a1/a2 to the average of d2/d1 is applied, the difference is not large for a1/a2 while it makes a large difference for a1/a3 as can be seen when comparing histograms 10f and 10e. When using only the calls within the 1.5 km limit from the center of the triplet and eliminating outliers (residuals of $|a1/a2-d2/d1|$ more than 1 and $|a1/a3-d3/d1|$ more than 2), the biases change to respectively 1.03 for a1/a2, and 1.37 for a1/a3. If the larger bias observed at S3 originates from the need to adjust the calibration of that hydrophone, it should be possible to observe the same kind of average differences for hydroacoustic arrivals propagating horizontally on large distances before reaching the triplet, of which there is a very large database at the IDC. This is however beyond the scope of this study.

Figure 11 shows a spatial mapping of the residuals. Panel 11a displays a1/a2-d2/d1 with lower absolute values of the residuals, slightly negative values around S1, and slightly positive values midway between S1 and S2. The a1/a3-d3/d1 residuals show an apparent positive slope roughly from S3 to the S1-S2 line (Figure 11b). A possible explanation for the discrepancies observed in the residuals in Figure 11b is that the S3 hydrophone's position is not correct and that it is located further away from the S1-S2 line than the coordinates used in this study indicate. Testing this hypothesis for a point located as shown on Figure 11d as S3', it is found that the constant bias is indeed removed from the distribution for point S3' at coordinates (-2.04km, -1.96km, S3 hydrophone depth unchanged) on the S1-S3 line at a distance 1.4 times larger than the distance S1-S3.

 doi:10.20944/preprints202410.1227.v1

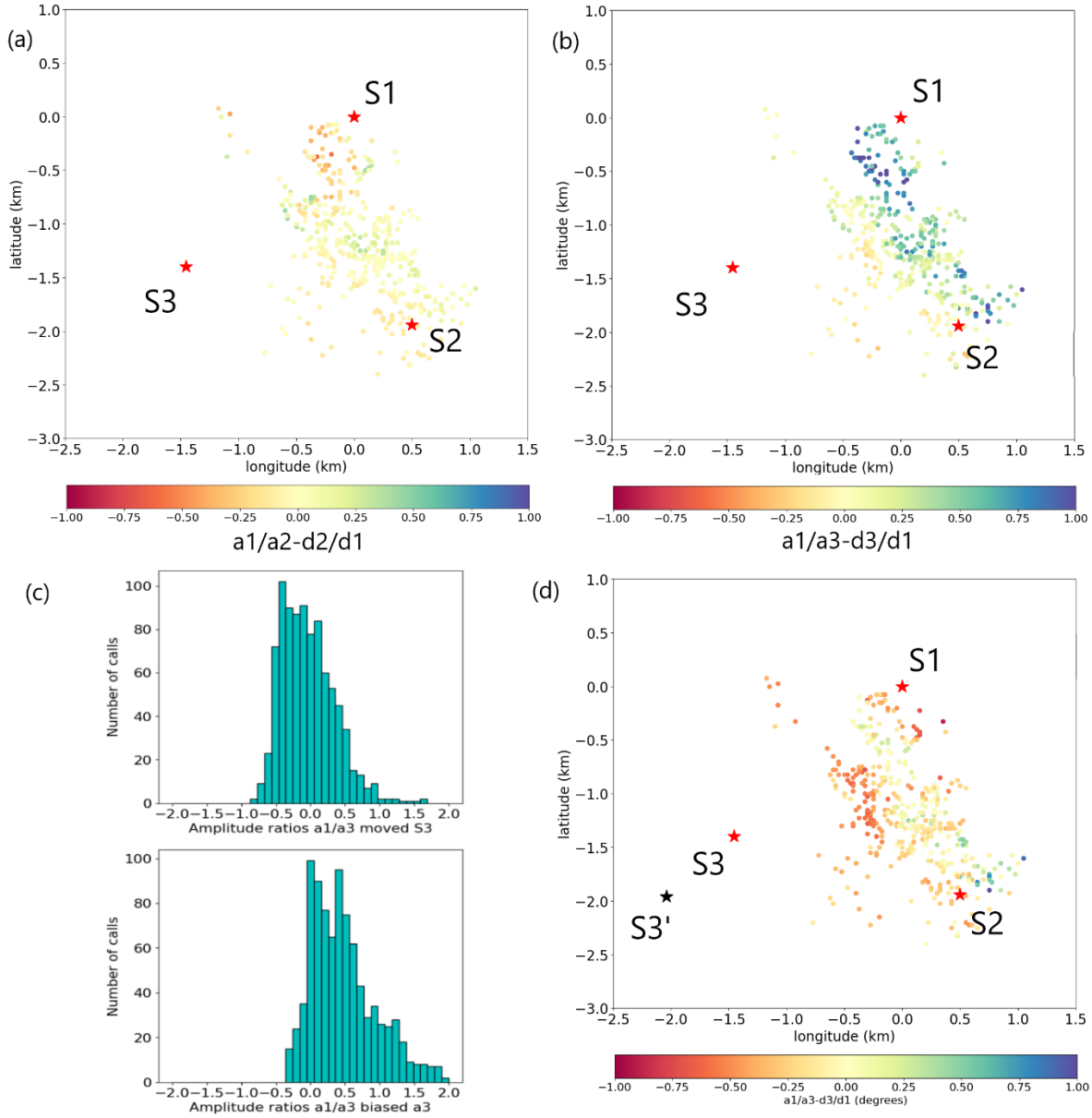

Figure 11. Spatial mapping of residuals a1/a2-d2/d1 (a) and a1/a3-d3/d1 (b). Note the higher amplitudes of the residuals in (b), which a plane sloping from the S1-S2 line towards S3 would fit. (c) Histograms of the a1/a3-d3/d1 residuals with original S3 (bottom) and moved S3′ (top). (d) Residuals a1/a3-d3/d1 when S3 is moved to S3′.

The standard deviation of residuals after moving the location of S3 to S3′ is higher than when a constant bias correction on S3 amplitudes is applied. One also has to keep in mind that the calculation of the vocalization locations itself depends on the location of S3, and that these locations have not been updated in this work before re-calculating the residuals.

3.2. Taking Advantage of Dense Coverage Close to S1 and S2 to Estimate Depths

The amplitude bias between S1 and S2 seems to be minimal, and therefore it should be possible to compare amplitudes of received calls with locations directly above the hydrophones. In that case, the distance to the closest hydrophone is the depth difference between the vocalization and the hydrophone. Assuming that the calls have the same source levels, and that the depth of the source is similar, the relative amplitudes a1/a2 at S1 should be similar to the relative amplitudes a2/a1 at S2.

 doi:10.20944/preprints202410.1227.v1

Figure 12a shows a map of call locations with a circle of 1.5 km in radius and circles of 250 m in radius around each of the three hydrophone locations.

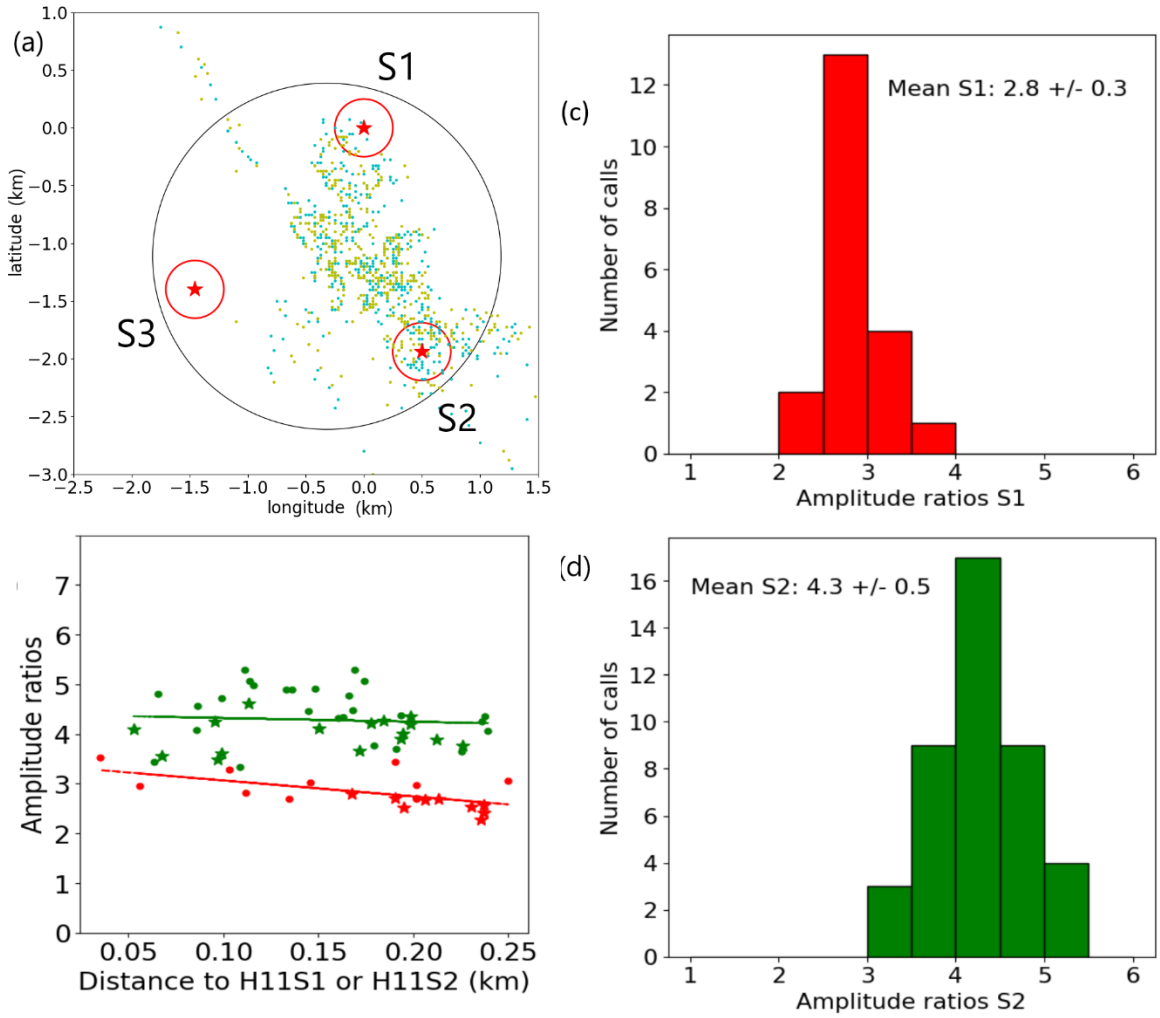

Figure 12. (a) Map of all calls analyzed in the study. A calls are in cyan, B calls in yellow. The large circle is centered in the middle of the triplet and has a radius of 1.5 km. The small red circles are centered on each hydrophone and have a radius of 250 m. (b) Amplitude ratios a1/a2 in red, and a2/a1 in green, displayed as a function of distance for calls within 250 m of the hydrophones. (c) Histogram of the amplitude ratios a1/a2 for calls close to S1. (d) Histogram of the amplitude ratios a2/a1 for calls close to S2.

The relative ratios a1/a2 are shown in red on Figure 12b for the calls within the 250 m circle at S1, and a2/a1 are shown in green for the calls within the 250 m circle at S2, for a passage of the whale between 23:40 on the 19 February and 00:40 on the 20 February. 'A' calls are marked as dots while 'B' calls are marked as stars. When the values published in [16] are used for the hydrophone depths, a ratio of:

$\frac{a1}{a2} = \frac{d2}{d1} = \frac{\sqrt{(h2-w)^2+D^2}}{h1} = \frac{\sqrt{0.55+4}}{0.75} = 2.84$ would be expected for a whale depth, w=0m, at the surface, where h1 and h2 are the hydrophone depths of respectively S1 and S2 and D is the horizontal distance between them, which is 2km. For w=20m:

$\frac{a1}{a2} = \frac{d2}{d1} = \frac{\sqrt{(h2-w)^2+D^2}}{h1-w} = \frac{\sqrt{0.521+4}}{0.73} = 2.91$

Figure 12b does indeed show that a ratio of 2.8 ± 0.3 is measured close to S1, which is compatible with the above estimates using distances, and the linear fit extrapolates to a value of 3.39 at S1, from which a value of 135m for the depth of vocalization of the whale can be derived. With the standard deviation of 0.3 for the ratio, the vocalization depth interval is 70m to 190m.

Conversely, at S2, the amplitude ratio would be expected to be:

 doi:10.20944/preprints202410.1227.v1

$\frac{a2}{a1} = \frac{d1}{d2} = \frac{\sqrt{(h1-w)^2+D^2}}{h2} = \frac{\sqrt{0.56+4}}{0.742} = 2.88$ at the surface,
and $\frac{a1}{a2} = \frac{d2}{d1} = \frac{\sqrt{(h1-w)^2+D^2}}{h2-w} = \frac{\sqrt{0.533+4}}{0.722} = 2.95$ for w=20m.

This is to be compared with the measured value of 3.8 ± 0.9 at S2, and in this case, there is a discrepancy between the theoretical (from distance ratios) and observed values. The linear fit extrapolates to 4.40 at S2, meaning a value of 255m for the depth. One possible explanation is that the vocalization depths is larger when it is close to S2. If a value of 0.5 is used for the standard deviation, the depth interval estimate is 190m to 305m.

Depths of the S1 and S2 hydrophones may have evolved since they were measured at respectively 750m and 724m. For instance, assuming that S1 is now at a depth of 855m, the values measured would account for a vocalization depth of 250m when in the vicinity of S1 and S2.

4. Discussion

Waveforms originating from vocalizing whales recorded on the IMS hydro acoustics station H11 have been presented and analysed for the possibility to localize the whales by time-of-arrival differences on each hydrophone in the station. The waveforms recorded for each whale-call on each hydrophone are rendered complex by the presence of the water surface reflection and multiple water bottom reflections. This leads to issues with methods based purely on waveform cross-correlation to estimate delays between hydrophones for signals like the ones studies in this work, which propagate mostly vertically when close to the hydrophone in horizontal distance. It occurs that some reflections are as energetic as the first, direct arrival, causing confusion as to which peak in the cross-correlation functions are to be used. The measurement of the amplitudes is also affected by the multiplicity of the arrivals, and perhaps a more sophisticated method than the one used in this study could be used to pick the amplitude of the first arrival with confidence, rather than assuming it will be the highest value of amplitude within a six second segment.

The results shown in this paper are inconclusive regarding the depth of the vocalizations, partly because analysis of the amplitudes cast some doubt on the exact value of the hydrophone depths. It should be possible to extract the waveform of the original signal by assuming a spectral shape, pitch variation, and minimum phase for each of the 'A' and 'B' types of call, using wavelet deconvolution techniques from the seismic exploration industry. Waveform modeling using a method that identifies individual arrivals, such as ray methods, should then become feasible, leading to estimations of the reflection coefficients and more exact whale depths estimates.

The location results shown in this paper are relying on the exactitude of the location and depths of the hydrophones. It is likely that there are in fact differences of possibly a few tens of meters between the depths of the three hydrophones, as the mooring cable lengths were pre-established during deployment, but the exact water depth at which the hydrophones were dropped is likely to have deviated from the depth of the target locations, even though a very precise bathymetry was acquired before the deployment. Analysis of the amplitudes of the signals exploited in this work points to a possible underestimate of the depths of S1, and a possible need for either correcting the S3 location to a point further from S1 and S2 or taking into account a possible calibration correction of the hydrophone at S3. A simple study of a large number of horizontally propagating signal recorded at the triplet should be able to confirm or infirm a calibration issue. In analyzing the amplitude of the signals, the assumption was made that the source of sound is spherically symmetrical, with no azimutally or vertically dependent radiation pattern. It may be possible, in a more refined analysis, to use the direction of motion of the whale as a substitute for the position of the animal and detect any variation in the strength of the signal depending on the position of the receiver with respect to the whale and its front to rear axis.

It may be possible to set up an inversion problem using both amplitudes and delay residuals to estimate potential corrections to the hydrophone locations. Early attempts at doing so using the locations derived from the delays and the residuals from the amplitudes yield unrealistically large corrections. One would have to assume that the average depth of vocalization is the same or similar

 doi:10.20944/preprints202410.1227.v1

throughout the sequence studied in this work. It would also be beneficial to search the data for additional similar sequences, providing better coverage especially close to the S3 hydrophone.

5. Conclusions

The sequence of calls studied in this work has a long duration and the tracks followed by the whale allow for a good coverage of the area directly above the triplets. It was shown that using the amplitudes of the signal when the source is in the near field confirms that they follow the expected 1/R decay rule, as opposed to the signals propagating horizontally.

A study of the residuals of observed amplitude ratios minus distance ratios and of the amplitude ratios when the whale is in the immediate proximity of hydrophones S1 on one hand and S2 on the other hand leads to the belief that corrections may be needed to the depths of the hydrophones.

Author Contributions: Conceptualization, R.L.B. and P.N.; methodology, R.L.B.; software, R.L.B.; formal analysis, R.L.B.; data curation, R.L.B.; writing—original draft preparation, R.L.B.; writing—review and editing, P.N.; All authors have read and agreed to the published version of the manuscript.

Funding: This research received no external funding

Data Availability Statement: The data from IMS hydroacoustic station HA11 is open available at the IRIS data center [17]. The data from HA01 as shown on Figure 1 can be obtained via the vDEC [24] mechanism of the CTBTO.

Acknowledgments: We are grateful to the senior management of CTBTO for allowing publication of [10], partly reproduced in this paper.

Conflicts of Interest: The authors declare no conflicts of interest.

References

1. International Whaling Commission. https://iwc.int/about-whales (last accessed 7 July 2024).
2. Thode, Aaron. (2004). Tracking sperm whale (Physeter macrocephalus) dive profiles using a towed passive acoustic array. The Journal of the Acoustical Society of America. 116. 245-53. 10.1121/1.1758972.
3. Thode, A. M., Kim, K. H., Blackwell, S. B., Greene, C. R., Nations, C. S., McDonald, T. L., et al. (2012). Automated detection and localization of bowhead whale sounds in the presence of seismic airgun surveys. *J. Acoust. Soc. Am.* 131, 3726–3747. doi:10.1121/1.3699247
4. Miksis-Olds, J. L., Harris, D. V., and Heaney, K. D. (2019a). "Comparison of estimated 20-Hz pulse fin whale source levels from the tropical Pacific and Eastern North Atlantic Oceans to other recorded populations," J. Acoust. Soc. Am. 146(4), 2373–2384.
5. Harris, D. V., Miksis-Olds, J. L., Vernon, J. A., and Thomas, L. (2018). "Fin whale density and distribution estimation using acoustic bearings derived from sparse arrays," J. Acoust. Soc. Am. 143(5), 2980–2993.
6. Balcazar, Naysa E., Joy S. Tripovich, Holger Klinck, Sharon L. Nieukirk, David K. Mellinger, Robert P. Dziak, Tracey L. Rogers, Calls reveal population structure of blue whales across the southeast Indian Ocean and the southwest Pacific Ocean, *Journal of Mammalogy*, Volume 96, Issue 6, 24 November 2015, Pages 1184–1193, https://doi.org/10.1093/jmammal/gyv126
7. Gavrilov, A. N., & McCauley, R. D. (2013). Acoustic detection and long-term monitoring of pygmy blue whales over the continental slope in southwest Australia. The Journal of the Acoustical Society of America, 134(3), 2505-2513.
8. Gavrilov, A. N., McCauley, R. D., Salgado-Kent, C., Tripovich, J., & Burton, C. (2011). Vocal characteristics of pygmy blue whales and their change over time. The Journal of the Acoustical Society of America, 130(6), 3651-3660.
9. Le Bras, Ronan J., Heidi Kuzma, Victor Sucic, Götz Bokelmann; Observations and Bayesian location methodology of transient acoustic signals (likely blue whales) in the Indian Ocean, using a hydrophone triplet. J. Acoust. Soc. Am. 1 May 2016; 139 (5): 2656–2667. https://doi.org/10.1121/1.4948758
10. Le Bras, Ronan J. and Peter Nielsen, (2017), Range estimates of whale signals recorded by triplets of hydrophones, AGU Fall Meeting. https://doi.org/10.1002/essoar.82a232e13a253c3f.ded9bfffb4b54848.1

11. Sirovic, A., Hildebrand, J. A., & Wiggins, S. (2007). Blue and fin whale call source levels and propagation range in the Southern Ocean. Journal of the Acoustical Society of America, 122(2), 1208-1215. https://escholarship.org/uc/item/8mr3c6vn
12. Kuna, V. M., John L. Nábělek, Seismic crustal imaging using fin whale songs. Science 371,731-735(2021). https://doi.org/10.1126/science.abf3962
13. Stimpert, A.K., DeRuiter, S.L., Falcone, E.A. et al. Sound production and associated behavior of tagged fin whales (Balaenoptera physalus) in the Southern California Bight. Anim Biotelemetry 3, 23 (2015). https://doi.org/10.1186/s40317-015-0058-3
14. Pereira, A., Danielle Harris, Peter Tyack, Luis Matias, 2020, On the use of the Lloyd's Mirror effect to infer the depth of vocalizing fin whales. J. Acoust. Soc. Am. 1 November 2020; 148 (5): 3086–3101. https://doi.org/10.1121/10.0002426
15. Lloyd, Humphrey (1831). "On a New Case of Interference of the Rays of Light". The Transactions of the Royal Irish Academy. 17. Royal Irish Academy: 171–177. ISSN 0790-8113. JSTOR 30078788. Retrieved 2021-05-29.
16. Zhu, J., Wen, L. (2024), Hydroacoustic study of fin whales around the Southern Wake Island: Type, vocal behavior, and temporal evolution from 2010 to 2022, J. Acoust. Soc. Am. 155, 3037–3050. https://doi.org/10.1121/10.0025776
17. Various Institutions. (1965). International Miscellaneous Stations [Data set]. International Federation of Digital Seismograph Networks. https://doi.org/10.7914/vefq-vh75
18. Lawrence, M., G. Haralabus, M. Zampolli, D. Metz, (2024). Comprehensive Nuclear-Test-Ban Treaty Organization, Vienna, (2024). The Comprehensive Nuclear-Test-Ban Treaty Hydroacoustic Network, *in* Kalinowski, M.B., Haralabus, G., Labak, P., Mialle, P., Sarid, E., Zampolli, M. (eds); Published by the Provisional Technical Secretariat of the Preparatory Commission for the Comprehensive Nuclear-Test-Ban Treaty Organization, Austria.https://www.ctbto.org/sites/default/files/2024-07/20240618-CTBTO%2025th%20Anniversary%20booklet%20Final%20HRes.pdf (last accessed 8/8/2024).
19. Allen R.V. (1978), Automatic earthquake recognition and timing from single traces, *Bull. seism. Soc. Am.* 68 1521, 1532
20. Trnkoczy A. (2002), Understanding and parameter setting of STA/LTA trigger algorithm *IASPEI New Manual of Seismological Observatory Practice* 2 01 20 Bormann P., doi:10.2312/GFZ.NMSOP-2_IS_8.1
21. Le Bras, R. J., P. Mialle, N. Kushida, P. Bittner, P. Nielsen, (2024). Developments in Hydroacoustic Processing for Nuclear Test Explosion Monitoring, *in* Kalinowski, M.B., Haralabus, G., Labak, P., Mialle, P., Sarid, E., Zampolli, M. (eds); Published by the Provisional Technical Secretariat of the Preparatory Commission for the Comprehensive Nuclear-Test-Ban Treaty Organization, Austria.https://www.ctbto.org/sites/default/files/2024-07/20240618-CTBTO%2025th%20Anniversary%20booklet%20Final%20HRes.pdf (last accessed 8/8/2024).
22. Cansi, Y. and Le Pichon, A. (2009) Infrasound Event Detection Using the Progressive Multi-Channel Correlation Algorithm. Handbook of Signal Processing in Acoustics, Springer, New York, 1425-1435.
23. Braving storms. Constructing hydroacoustic station HA11 Wake Island. https://www.ctbto.org/news-and-events/news/braving-storms-constructing-hydroacoustic-station-ha11-wake-island (last accessed 22/7/2024)
24. VDEC. https://www.ctbto.org/resources/for-researchers-experts/vdec (last accessed 10/7/2024).